Wideband Tunable Idler Filtering in a Monolithically Integrated Silicon Photonic Wavelength Converter

Hao Liu[(1,*)], Kyle R.H. Bottrill[(1)], Valerio Vitali[(1,2)], Iosif Demirtzioglou[(1,3)], Nura Adamu[(1)], Cosimo Lacava[(1,2)], Xingzhao Yan[(1)], Mehdi Banakar[(1)], Ying Tran[(1)], Martin Ebert[(1)], James Le Besque[(1)], Callum LittleJohns[(1)], David J. Thomson[(1)] and Periklis Petropoulos[(1)]

[(1)] Optoelectronics Research Centre, University of Southampton, Southampton, SO17 1BJ, UK, [*]hl19n23@soton.ac.uk
[(2)] Electrical, Computer and Biomedical Engineering Department, University of Pavia, Pavia, 27100, Italy,
[(3)] Currently at: Huawei Technologies, Paris Research Center, Optical Communication Technology Lab, 92100 Boulogne-Billancourt, France.

Abstract *We present a silicon photonic wavelength converter and integrated filter achieving wideband tunable filtering over 25 nm with a >52 dB pump and modulated signal suppression ratio. Operation of the device with telecommunication signals is demonstrated across the C-band. ©2024 The Author(s)*

Introduction

All-optical wavelength conversion, extensively researched in recent decades, holds the potential to enable flexible traffic growth and alleviate wavelength contention, thereby enhancing overall spectrum utilization[1]. Four-wave mixing (FWM) in $\chi^{(3)}$ media, such as highly nonlinear fibre[2][3], silicon[4][5], silicon nitride[6][7], and AlGaAsOI[8], can offer broad bandwidth and modulation format transparency at high data rates, rendering it a promising enabler. Integrated nonlinear wavelength converters built on the silicon-on-insulator (SOI) platform hold promise, benefiting from the strong optical confinement provided by the high refractive index of silicon[4][5].

Typically, the converted idler generated in FWM-based wavelength converters will necessitate additional off-chip filtering to suppress the high-power pump and original signal at the device output[9]. The high Kerr coefficient of silicon, combined with its high thermal sensitivity make it possible to realize wavelength conversion, wideband tunable idler filtering, and effective suppression of undesired signals on the same platform. FWM-based wavelength conversion in silicon photonic microring resonators, along with on-chip idler filtering and suppression of undesired signals, has been shown in the literature[10][11], but without demonstrating tunable filtering. Therefore, the placement of the signal wavelengths in these demonstrations was limited by the resonance wavelength position of the microring resonator. Recently, we investigated the tunable idler filtering and suppression of the pump and signal in FWM-based wavelength converters in[12]. However, this demonstration was hindered by the heater design within the characterized structures, which was unable to achieve a thermally-induced 2π phase shift in each resonator. Thus, it was not possible to achieve wideband and dense tuning of the resonance wavelength. Consequently, we could not demonstrate individual selection of idler channels using the on-chip filter while continuously tuning the signal wavelength across the device's operating region, which is necessary to prove the practicality of such devices in telecommunications scenarios.

In this work, we initially present the conversion efficiency (CE) spectrum of the PN-junction equipped silicon waveguide and characterise the filter for its capability for wide, precise and continuous tuning. Then, by utilising a 16-QAM, 32 Gbaud single polarization signal tuned to three selected channels, we demonstrate channel-to-channel conversions spanning approximately 25

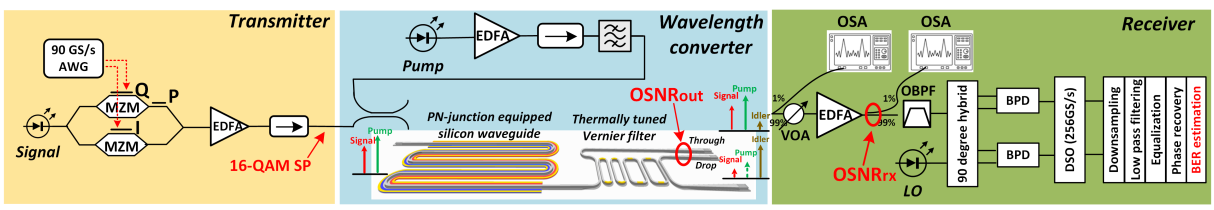

Fig. 1: System setup of coherent transmitter, wavelength converter, and coherent receiver. Arbitrary waveform generator (AWG); Mach-zehner modulator (MZM); Erbium-doped fibre amplifier (EDFA); Optical bandpass filter (OBPF); Optical spectrum analyzer (OSA); Local oscillator (LO), Variable optical attenuator (VOA), Digital sampling oscilliscope (DSO); Balanced photodetector (BPD)

nm. We present bit error ratio (BER) measurements of the generated idlers to identify the main source of conversion penalties in this device configuration. Our results demonstrate wideband and dense tuning, achieving an approximately 60 dB extinction ratio (ER) between the minimum and maximum normalized transmission measured at the drop port, along with selective channel-to-channel conversions to provide $>$52 dB pump and modulated signal suppression ratio, all achievable in this device configuration.

Device description and experimental setup

The device layout and experimental setup are illustrated in Fig. 1. The device comprises a 1cm long PN-junction-equipped silicon rib serpentine-shaped waveguide, followed by a high-order thermally tuned Vernier filter. The PN-junction equipped silicon rib waveguide was designed with a 220nm waveguide height and 100nm slab thickness, with a distance of 0.8μm between the silicon waveguide core and the doped regions. The high-order Vernier filter was designed as a cascade of four silicon racetrack resonators to achieve a free spectral range (FSR) of approximately 40nm. A large FSR was necessary in order to achieve wideband tuning of the resonance wavelength. Tuning was achieved with individual 6 μm-wide metal heaters (Aluminum/Titanium stack) which were deposited on top of each racetrack resonator, allowing for thermally-induced phase shifts larger than 2π. The device was equipped with uniform grating couplers at its input and output, enabling robust coupling, but limiting the 3 dB bandwidth of device operation to between 1530 and 1578 nm.

The 32GBaud single-polarization 16-QAM signal was generated by modulating a tunable, C-band continuous-wave (CW) laser with an IQ modulator, which encoded a $2^{15}-1$ pseudo-random bit sequence (PRBS) generated from a 90GS/s Arbitrary waveform generator (AWG). Digital matched root-raised-cosine filtering was applied at both the transmitter and receiver stages. The modulated optical signal was amplified and coupled together with the pump. The pump was generated by a CW source, with its wavelength set at 1552.52 nm (Ch31), amplified by an erbium-doped fiber amplifier (EDFA), and filtered using an optical bandpass filter (OBPF) to reject out-of-band amplified spontaneous emission (ASE). At the output of the device, the filtered idler and any residual pump and signal were collected at the drop port of the high-order Vernier filter and sent to a pre-amplified coherent

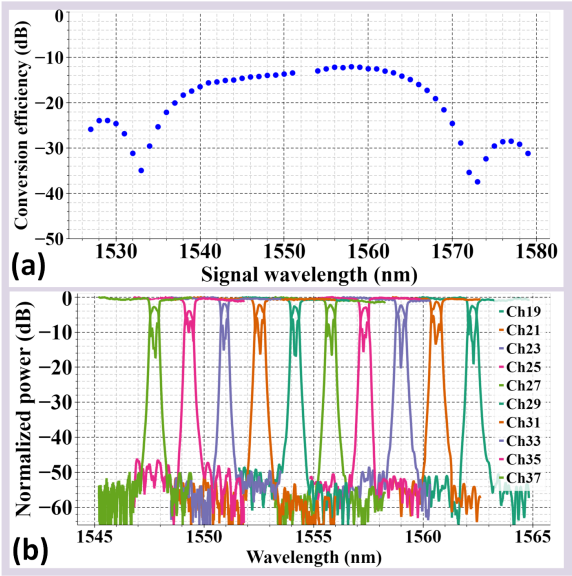

Fig. 2: (a) Conversion efficiency spectrum; (b) Normalized through and drop port responses aligned to ITU-T grid with 200 GHz channel spacing (Ch19-Ch37).

receiver. This receiver consisted of a narrow optical band-pass filter to reject the undesired ASE, followed by a digital storage oscilloscope (DSO) operating at 256 GSa/s. Offline digital signal processing (DSP) enabled demodulation and BER measurements via bit error counting.

Results and Discussion

Utilizing a simplified version of the setup of Fig. 1, we first measured the CE spectrum using a PN-junction equipped silicon rib waveguide without an on-chip filter, as depicted in Fig. 2(a). The input pump power into the waveguide was approximately 24 dBm, accounting for a measured 4.65 dB loss per grating coupler. A maximum of -11 dB on-chip CE was achieved when the signal wavelength was approximately 3 nm away from the pump wavelength, with lower CE values observed as the signal wavelength moved towards shorter wavelengths. The asymmetric CE spectrum arises from the wavelength response of the grating coupler, which has its transmission peak at 1555 nm.

Subsequently, the characterization results of the high-order Vernier filter, utilizing two cascaded EDFAs to reveal the full ER of the filter are shown in Fig. 2(b), and demonstrate effective tuning of the resonance wavelength of the Vernier, racetrack resonator-based filter, aligning them within the channel range Ch19 - Ch37. It should be noted that the demonstration of the resonance wavelength tuning is limited by the gain bandwidth of the EDFAs. An ER of around 60 dB measured at the drop port was achieved, with an insertion loss measured at the drop port in the range of 1-4 dB.

Variations in ER and insertion loss across different channels can be attributed to coupling coefficient variations between each racetrack resonator due to thermal crosstalk in the heater actuation.

Finally, we carried out channel-to-channel conversions of a 32 Gbaud 16-QAM modulated signal using the system setup shown in Fig.1. With the pump wavelength held constant at Ch31, we set the signal wavelengths at Ch28, Ch38.5, and Ch47, to result in idler generated at Ch34, Ch23.5, and Ch15, respectively, as shown in Fig.3(a)-(c). These three channels represent examples of signal wavelengths placed both close and further away from the pump. Ch47 in particular, was chosen to represent an extreme case. Here, the signal is placed near the CE spectrum edge, where the OSNR is just high enough idler to ensure a measurable BER. Ensuring that the resonance wavelengths of each racetrack resonator were aligned with the idlers of the three measured channels, we acquired the FWM spectra at both the through and drop ports. For easier comparison and to facilitate evaluation of the suppression of undesired signals, we present the measurements taken at the drop port (in red) in Fig.3(a)-(c), together with corresponding through-port measurements (in blue), where the signal wavelength is detuned by 0.5 nm.

The resultant spectra demonstrate effective suppression of both the modulated signal and pump (>58.2 dB) for signal wavelengths positioned at Ch28 and Ch38.5, as shown in Fig. 3(a)(b). When the signal is positioned at Ch47, one of the suppressed resonant peaks of the high-order Vernier filter partially overlaps with the pump, resulting in a lower, 52dB suppression ratio (Fig. 3(c)). In addition, the idler-to-residual pump power ratio is maintained at approximately 30 dB in Fig. 3(a)(b), while only showing 20 dB in Fig. 3(c). This decrease can be attributed to the decrease in CE at shorter wavelengths, resulting in a reduction in the optical signal-to-noise ratio (OSNR) of the converted idler measured at the through ports, as shown in Fig. 3(a)-(c). This also corresponds to a significant increase in conversion penalties evaluated at the HD-FEC limit (black dashed line), as depicted in Fig. 3(d). A 9 dB power penalty is observed when converting Ch47, as opposed to 1-3.5 dB for Ch28 and Ch38.5. These observations highlight the importance of achieving a high idler OSNR before the high-order Vernier filter as it ensures the maintenance of a high idler-to-residual pump ratio and the simultaneous minimization of conversion penalties.

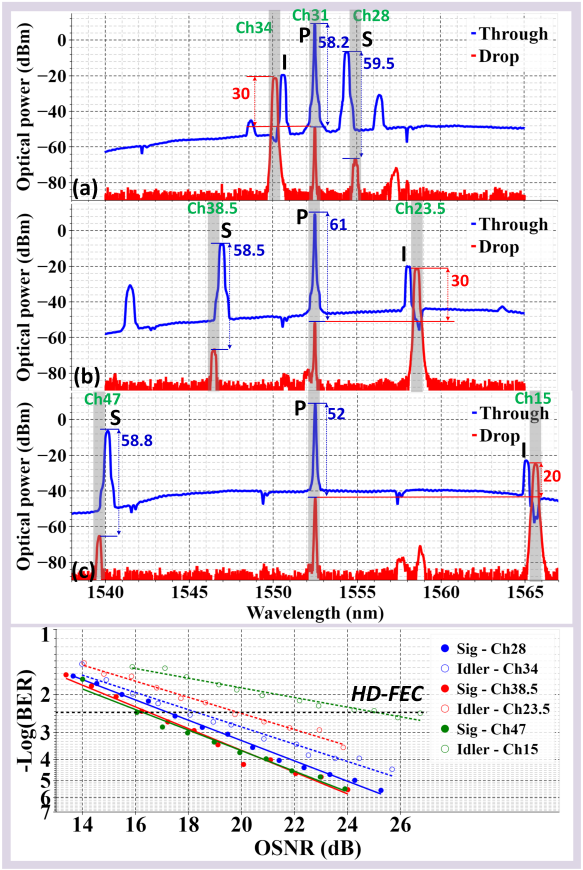

Fig. 3: FWM spectra measured at the through (off-resonance) and drop (on-resonance) output ports with signal wavelengths respectively at (a) Ch28, (b) Ch38.5, and (c) Ch47; (d) BER measurements with three back-to-back channels and three wavelength converted channels.

Conclusions

We characterized a silicon photonic wavelength converter integrated with a high-order Vernier filter, offering wideband and continuously tunable resonance wavelengths with approximately 60 dB ER. Effective suppression of the undesired modulated signal and strong pump, exceeding 52 dB, is achieved across the three selected channels spanning approximately 25 nm, while maintaining the best idler-to-residual-pump power ratio of around 30 dB. Channel-to-channel conversion over a larger wavelength span and achieving a higher idler-to-residual-pump power ratio are possible through proper dispersion engineering and the utilization of lower-loss silicon photonic waveguides. As a future development, we envision the realization of more efficient wavelength converters that can be extended to other optical communication bands, equipped with highly effective on-chip filtering capabilities and more efficient coupling strategies[13] to enhance the CE further. These advancements pave the way for future large-scale integration of all-optical signal processing capabilities on-chip.

Acknowledgements

This work was supported by the UK's EPSRC through grants (EP/T007303/1 and EP/T019697/1) and the DSIT project REASON. The data for this work is accessible through the University of Southampton Institutional Research Repository DOI:/10.5258/SOTON/D3055.

References

[1] A. A. Saleh and J. M. Simmons, "All-optical networking—evolution, benefits, challenges, and future vision", *Proceedings of the IEEE*, vol. 100, no. 5, pp. 1105–1117, 2012. DOI: 10.1109/JPROC.2011.2182589.

[2] H. Liu, K. R. Bottrill, A. Masoudi, V. Vitali, and P. Petropoulos, "Reflectometric measurements of fibre-based four-wave mixing systems", *Journal of Lightwave Technology*, 2023.

[3] K. R. Bottrill, N. Taengnoi, H. Liu, R. Kakarla, Y. Hong, and P. Petropoulos, "Suppression of spurious mixing in fwm-based systems through mid-span pump phase shift", in *Optical Fiber Communication Conference*, Optica Publishing Group, 2022, W4J–2.

[4] A. Gajda, L. Zimmermann, M. Jazayerifar, *et al.*, "Highly efficient cw parametric conversion at 1550 nm in soi waveguides by reverse biased pin junction", *Optics express*, vol. 20, no. 12, pp. 13 100–13 107, 2012. DOI: 10.1364/OE.20.013100.

[5] F. Da Ros, A. Gajda, E. Liebig, *et al.*, "Dual-polarization wavelength conversion of 16-qam signals in a single silicon waveguide with a lateral pin diode", *Photonics research*, vol. 6, no. 5, B23–B29, 2018. DOI: 10.1364/PRJ.6.000B23.

[6] V. Vitali, T. D. Bucio, H. Liu, *et al.*, "Fully integrated and broadband si-rich silicon nitride wavelength converter based on bragg scattering intermodal four-wave mixing", *Photonics Research*, vol. 12, no. 3, A1–A10, 2024. DOI: 10.1364/PRJ.506691.

[7] P. Zhao, Z. He, V. Shekhawat, M. Karlsson, and P. A. Andrekson, "100-gbps per-channel all-optical wavelength conversion without pre-amplifiers based on an integrated nanophotonic platform", *Nanophotonics*, vol. 12, no. 17, pp. 3427–3434, 2023. DOI: 10.1515/nanoph-2023-0264.

[8] M. Pu, H. Hu, L. Ottaviano, *et al.*, "Ultra-efficient and broadband nonlinear algaas-on-insulator chip for low-power optical signal processing", *Laser & Photonics Reviews*, vol. 12, no. 12, p. 1 800 111, 2018. DOI: 10.1002/lpor.201800111.

[9] P. M. Kaminski, F. Da Ros, E. P. da Silva, *et al.*, "Characterization and optimization of four-wave-mixing wavelength conversion system", *Journal of Lightwave Technology*, vol. 37, no. 21, pp. 5628–5636, 2019. DOI: 10.1109/JLT.2019.2933226.

[10] J. R. Ong, R. Kumar, and S. Mookherjea, "Silicon microring-based wavelength converter with integrated pump and signal suppression", *Optics letters*, vol. 39, no. 15, pp. 4439–4441, 2014. DOI: 10.1364/OL.39.004439.

[11] G. Cantarella, C. Klitis, M. Sorel, and M. J. Strain, "Silicon photonic filters with high rejection of both te and tm modes for on-chip four wave mixing applications", *Optics Express*, vol. 25, no. 17, pp. 19 711–19 720, 2017. DOI: 10.1364/OE.25.019711.

[12] H. Liu, K. Bottrill, V. Vitali, *et al.*, "Fully-integrated silicon wavelength converter with on-chip idler filtering", *CLEO*, 2024.

[13] V. Vitali, T. D. Bucio, C. Lacava, *et al.*, "High-efficiency reflector-less dual-level silicon photonic grating coupler", *Photonics Research*, vol. 11, no. 7, pp. 1275–1283, 2023.